Interactive regulation between aliphatic hydroxylation and aromatic hydroxylation of thaxtomin D in TxtC, a theoretical investigation

Chang Yuan, Qingwen Ouyang, Hongwei Tan*, Guangju Chen* and Xichen Li

College of Chemistry, Key Laboratories of Theoretical and Computational Photochemistry, Ministry of Education, Beijing Normal University, Beijing, China.

Corresponding Authors:

Hongwei Tan*,

Email: hongwei.tan@bnu.edu.cn,

ABSTRACT

TxtC is an unusual bifunctional Cytochrome P450 which is able to perform sequential aliphatic and aromatic hydroxylation of the diketopiperazine substrate thaxtomin D in two remote sites to product thaxtomin A. Though the X-ray structure of TxtC complexed with thaxtomin D revealed a binding mode for its aromatic hydroxylation, the preferential hydroxylation site is aliphatic C_{14}-H. It is thus intriguing to unravel how TxtC accomplishes such two-step catalytic hydroxylation on the distinct aliphatic and aromatic carbons and why the aliphatic site is preferred in the first hydroxylation step. In this work, by employing molecular docking and MD simulation, we revealed that thaxtomin D could adopt two different conformations in the active site of TxtC which is equally in energy, with either the aromatic C-H or aliphatic C_{14}-H laying towards the active oxyferryl moiety of Cpd I. Further ONIOM calculations indicated that the energy barrier for the rate-limiting step of hydroxylation on the aliphatic C_{14} site is 8.9 kcal/mol favourable than that of on the aromatic C_{20} site. The hydroxyl group on the C_{14} site of the mono-hydroxylated intermediate thaxtomin B forms hydrogen bonds with Ser280 and Thr385, which induce the L-Phe moiety to rotate around the C_{β}–C_{γ} bond of 4-nitrotryptophan moiety significantly to adopt an energy favourable conformation with aromatic C_{20} in the adjacent of the oxyferryl moiety. Meanwhile, the hydroxyl group induces entrance of solvent water molecules in the active site, which propels the thaxtomin B to move towards the heme plane and results in distortion of heme. Based on this geometrical layout, the rate-limiting energy barrier of aromatic hydroxylation decreases to 15.4 kcal/mol which is comparable to that of the aliphatic hydroxylation process of thaxtomin D. Our calculation results indicated that the heme distortion lowers the energy level of the lowest α-vacant orbital of Cpd I, which promotes the electron transfer process of the rate-limiting step of thaxtomin B aromatic hydroxylation in TxtC.

INTRODUCTION

Thaxtomins (Thxs) are a family of phytotoxic diketopiperazines and causative agents of multiple plant pathogenic Streptomyces strains which inhibit cellulose biosynthesis in expanding plant tissues.[1,2] Thxs are often pursued as herbicides for crop protection due to their virulence.[3,4] However, the synthetic routes to Thxs suffered from the lack of stereo-control and low overall yield.[5,6] Recently, it was reported that TxtC is able to effectively produce thaxtomin A, an herbicide approved by the U.S Environmental Protection Agency (EPA),[3,4,7] from thaxtomin D. TxtC is a member from cytochrome

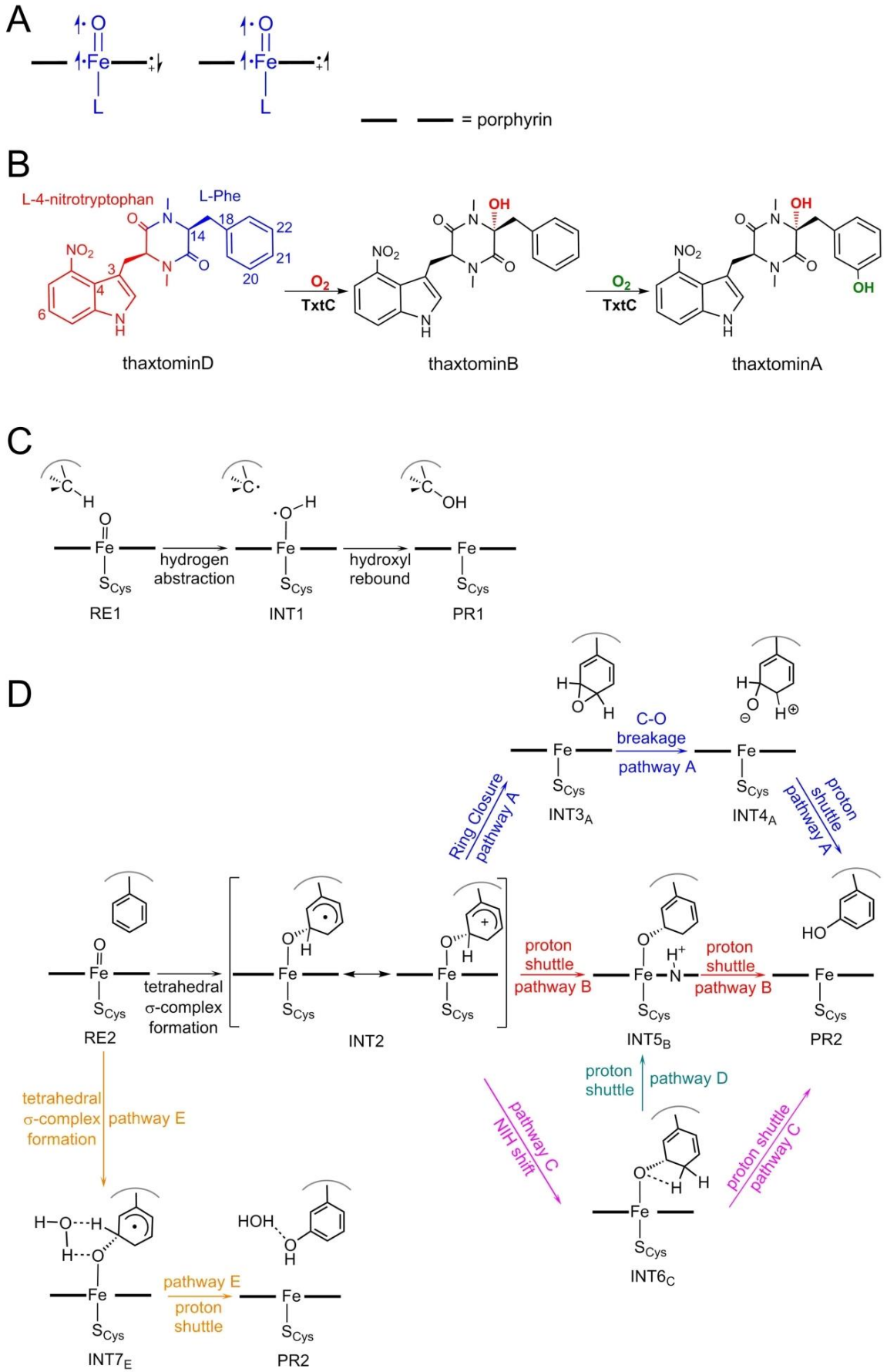

Scheme 1 (A) The sketch map of doublet and quartet active oxyferryl species. (B) Schematic outline of the thaxtomin A biosynthetic route, starting with the thaxtomin D, which is assembled from L-Phe and 4-nitrotryptophan. (C) Alternative mechanistic hypotheses for the aliphatic hydroxylation (C) and aromatic hydroxylation (D) by cytochromes P450s.

P450 family which consists of versatile monooxygenases to execute a broad array of biochemical transformations, such as, hydroxylation of alkane, oxidation of heteroatoms or aromatics, and dealkylation reactions.[8–12] In these catalytic reactions, the active high-valent iron-oxo porphyrin π-cation radical (Cpd I, as shown in Scheme 1A) species serves as the oxygen source. The conversion from thaxtomin D to thaxtomin A in TxtC is a two-step process. Firstly, Cpd I inserts an oxygen atom into the aliphatic C_{14}-H bond of thaxtomin D to generate thaxtomin B, which is followed by the second hydroxylation step on the meta-position of phenyl group of thaxtomin B to produce thaxtomin A[3,4,7] (see in Scheme 1B). It is worth noting that aliphatic and aromatic C-H bond usually have as high as 10 ~ 20 kcal/mol energy difference in the bond dissociation energies (BDE), which means that TxtC is able to use distinct strategies to accomplish the sequential aliphatic and aromatic hydroxylation on thaxtomin D. The catalytic hydroxylation mechanism of cytochrome P450 has been extensively investigated by both experimental and theoretical studies. As shown in Scheme 1C, aliphatic hydroxylation by cytochrome P450 follows a common mechanism which involves initial hydrogen atom abstraction (HAT) by Cpd I followed by hydroxyl rebounding.[13–18] While aromatic hydroxylation by cytochrome P450 is much more complicated.[16–20] Scheme 1D summarizes several mechanistic hypotheses for it. As one can see, all the mechanisms leading to hydroxylation on aromatic ring are channelled through a tetrahedral σ-complex intermediate (INT2 in Scheme 1D) formed by oxyferryl from Cpd I adding to the aromatic carbon of the substrate. The subsequent reaction process is proposed to proceed in different pathways. One of the proposed pathway (Pathway A, Scheme 1D) goes through an epoxide intermediate, which then converts to hydroxylation product by cleaving the bond between oxygen and the ortho-carbon being accompanied with 1,2-hydrogen shift (NIH shift)[21]. However, deuterium isotope experiment indicated that aromatic hydroxylation by cytochrome P450 is unlikely to follow such an epoxide formation mechanism.[22] An alternative aromatic hydroxylation mechanism via the tetrahedral σ-complex intermediate was proposed by Shaik et al[20] (Pathway B, Scheme 1D), in which the porphyrin ring acts like a springboard that mediates a proton shuttle from the tetrahedral carbon of the substrate to the oxygen atom of oxyferryl moiety through one of the pyrrole N in porphyrin ring. The proton migration from the tetrahedral carbon to the oxygen atom could also be accomplished through NIH shifting mode as shown by pathway C in Scheme 1D, in which the proton shuttle is mediated by ortho-carbon atom of the phenyl ring. So to speak, both aliphatic and aromatic

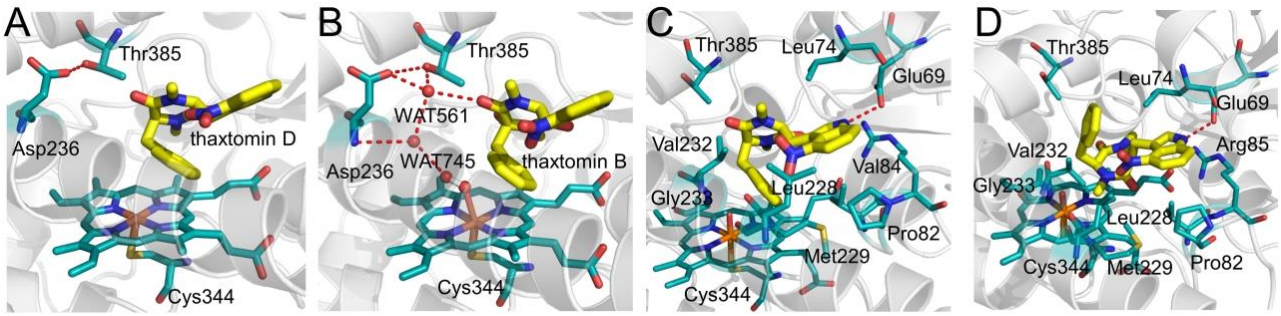

Figure 1 Active sites of cytochromes P450 TxtC combines with thaxtomin D (A, PDB code: 6f0b), thaxtomin B (B, PDB code: 6f0c) in the X-ray crystal structures. MD simulated complexes of TxtC-thaxtomin D in complex A (C) and complex B (D). The key residues in the active site are represented as sticks. Carbon, oxygen, sulfur and nitrogen atoms are coloured in cyan, red, orange and blue respectively. The carbon atoms in the substrate molecules are coloured in yellow. The H-bonds are represented as red dashed lines.

hydroxylation are well within the scope of activities of cytochrome P450, but how TxtC integrates these two activities in a single active centre is rarely known yet. Further effort is therefore desired to unravel the bifunctional hydroxylation mechanism of TxtC.

Recently, Challis et al determined the X-ray crystal structures of TxtC in complex with thaxtomin D (PDB code: 6f0b) and thaxtomin B (PDB code: 6f0c) respectively.[7] As shown in Figure 1A and 1B, the crystal structures revealed that heme functions as the prosthetic group in these two complexes, of which the iron cation connects to the protein backbone via the thiolate linkage of the distal Cys ligand (Cys344). It is interesting to note that in complex structures, thaxtomin D adopts a very similar conformation as thaxtomin B. Both of the two substrate molecules place the phenyl group in the vicinity of the oxyferryl moiety, though the preferential hydroxylation site of thaxtomin D is its aliphatic atom C_{14}. It therefore indicated that thaxtomin D should has an alternative conformation in TxtC's active site by placing C_{14} next to the catalytic iron centre. Docking calculations conducted by Challis et al. supported the speculation that the active site of TxtC can accommodate two distinct binding scenarios of thaxtomin D, in which either the phenyl group or aliphatic C_{14} of thaxtomin D lies over the heme plane respectively[7]. Given that TxtC displays clearly sequential hydroxylation of aliphatic C_{14} prior to the aromatic C_{20} on thaxtomin D, an intriguing question how TxtC realizes such regioselectivity thus raised. Several previous works have studied the regioselective oxidation reaction by cytochrome P450. As for the detoxification process of 1-methyl-4-phenyl-1,2,3,6-tetrahydropyridine (MPTP) by cytochrome P450 (mainly CYP2D6), theoretical calculation identified that its N-demethylation is thermodynamically more favourable than the aromatic hydroxylation process.[23] Experimental results from synthesized biomimetic iron–oxo porphyrin oxidants indicated that the proximal axial ligand of iron is an important factor for the oxidation regioselectivity. With

acetonitrile as the proximal ligand, [Fe^{IV}=O($Por^{+\cdot}$)$NCCH_3$] showed aromatic preferential in the ethylbenzene oxidation reaction, while [Fe^{IV}=O($Por^{+\cdot}$)Cl^-] predominantly produced the 1-phenylethanol as the oxidation product.[24] A follow-up DFT study revealed that the anionic axial ligand chloride weakens the electrophilicity of the oxidant so that the aromatic hydroxylation process, which depends on electron-transfer from the substrate to the oxidant, is significantly suppressed .[25] In addition, Shaik et al indicated that the hydrogen bonds formed around the axial thiolate ligand act as external electric field along the S-Fe-O axis and change the electronic conformation of Cpd I, thus dictate the regioselectivity between epoxidation and allylic hydroxylation of propene by Cpd I.[26] Generally speaking, as an active oxidant, Cpd I is acts a "chemical chameleon" owing to its maneuverable electronic structure in the different protein environments. However, whether and how the structural and electronic factors of TxtC determine its regioselectivity between aliphatic and aromatic hydroxylation of thaxtomin D are still elusive. As a matter of fact, TxtC performs aromatic hydroxylation on hydroxylated intermediate thaxtomin B instead of thaxtomin D, whether the hydroxyl moiety on C_{14} site of thaxtomin B influences the aromatic hydroxylation reaction process remains unknown. Actually, kinetic experiment determined that the aromatic hydroxylation efficiency of thaxtomin B is in the same order as that of the aliphatic hydroxylation on thaxtomin D in TxtC,[3] which infers that TxtC uses a mechanism which is not clear yet to regulate the two-step hydroxylation reactions.

In the present study, MD simulations and ONIOM calculations were employed to address the mechanistic details of sequential aliphatic and aromatic hydroxylation of thaxtomin D in TxtC. Our computational results revealed that the initial aliphatic C_{14}–H activation of the thaxtomin D proceeds via a rate-limiting HAT step with hydrogen atom on the C_{14} transferring to the oxoferryl of Cpd I, which is followed by the hydroxyl moiety rebound to generate the C_{14} hydroxylated intermediate thaxtomin B. The hydroxyl group on C_{14} site forms hydrogen bonds with Ser280 and Thr385, which induces isomerization of thaxtomin B to place the aromatic carbon (C_{20}) next to the oxyferryl moiety, which initiates the three-step aromatic hydroxylation of thaxtomin B: (1) the rate-limiting tetrahedral σ-complex intermediate formation with electron transfer from the thaxtomin B to Cpd I, (2) NIH shift, and (3) proton shuttling via porphyrin. Our ONIOM calculation and molecular dynamics simulation results show that the hydroxyl group of C_{14} of thaxtomin B plays crucial role in its aromatic hydroxylation process by inducing the entrance of bulk water molecules into the active pocket, which

propels thaxtomin B to move towards the heme plane and results in out-of-plane distortion of heme ring. Such a conformation change promotes the electrophilicity of Cpd I in TxtC so that it is able to perform aromatic hydroxylation on thaxtomin B facilely. This work revealed the critical role of hydroxyl moiety on the C_{14} site of thaxtomin B in steering its aromatic C-H hydroxylation and provided new insights into the interactive influence between the substrate and the activity of enzyme.

MODELS AND METHODS

The X-ray structure of TxtC-thaxtomin D complex showed that the substrate adopts an orientation with which Cpd I cannot perform hydrogen atom extraction from C_{14} site.[7] To obtain a proper starting structure of thaxtomin D complexed in TxtC for its aliphatic carbon hydroxylation, molecular docking was conducted based on the crystal structure of TxtC (PDB code: 6f0b)[7] by using the program AutoDock 4.2.[27] When performing the docking calculations, the protein TxtC was set to be rigid, while for the substrate thaxtomin D, all the C-C, C-N single bonds were set to be rotatable to better fit in the pocket. A cubic grid with 108*90*108 grid points and a spacing of 0.59 Å was chosen to ensure complete coverage of TxtC. The docking simulation was performed with 500 cycles using Lamarckian genetic algorithm (LGA).[28]

Docking calculations indeed gave out two optimal TxtC-thaxtomin D complex structures in which thaxtomin D places its phenyl group and aliphatic C_{14} next to the oxyferryl moiety respectively (Figure S1). These two complexes of TxtC-thaxtomin D and the TxtC-thaxtomin B complex (taken from X-ray structure with PDB code: 6f0c) were then submitted for further molecular dynamics (MD) simulations. The hydrogen atoms were added to the complex structures by using the PROPKA program[29] based on the experimental pH environment. Amber ff14SB force field[30] was used for the protein, while the substrate molecules thaxtomin D and thaxtomin B were parametrized by using the ANTECHAMBER module.[31,32] The force field parameters of heme oxyferryl complex (Cpd I) were taken from the literature[33]. The three complexes were soaked into TIP3P[34] water box with a minimum distance of 10 Å to the protein boundary and neutralized with counter ions Na^+ respectively. Each of the processed systems was then submitted to a three-step energy minimization for the hydrogen atoms, solvent molecules and the whole system respectively to relax the possible clashes. After energy minimization, the systems were then heated to 300 K and equilibrated for 300 ps. Finally, molecular

dynamic simulations were performed in the NPT ensemble for 100 ns to obtain the product phase. From each of the MD simulation trajectories, three independent and stable snapshots at 50, 80, 100 ns were abstracted and used to build the models for mechanism investigation with ONIOM approach.[35] Since the entire protein of TxtC is rather large, a truncated model which contains all the residues within 10 Å of the active site was built for ONIOM calculations. The QM region of the model consists of (1) the active oxidant Cpd I, (2) the thiolate cysteine residue (Cys344), which is the proximal ligand of iron centre, (3) the substrate (thaxtomin D/thaxtomin B). In the model of TxtC-thaxtomin B, two crystal water molecules (WAT561, WAT745) residing in the active site and having hydrogen bond interaction with Asp236 and Thr385 were also included. The QM-MM layer boundary was captured with hydrogen atoms. All the atoms in the MM region except those within 6 Å of QM zone were frozen during optimization. TAO toolkit[36] was employed in preparing the ONIOM calculations.

All the geometry optimizations including transition structure searches were performed by using ONIOM protocol, in which the DFT hybrid functional B3LYP[37] with def2-SVP[38] basis set was employed for all the atoms in the QM part, while AMBER ff98 force field[39] embedded in Gaussian 09 program[40] was used for the MM part. Intrinsic reaction coordinate (IRC) and harmonic vibrational frequency calculations were conducted at the same theoretical level of optimization to confirm that the correct stationary point structures were located. Zero-point energy (ZPE) and entropy corrections were obtained based on the frequency calculations. Van der Waals effect was assessed by using Grimme's D3 method.[41] Energy corrections with higher accuracy were then evaluated with ONIOM (electronic embedding) protocol by using B3LYP/def2-TZVP[42] for the QM atoms. All calculations were performed with Gaussian09 program package.[40]

RESULTS AND DISCUSSION

The target systems

As TxtC performs sequential hydroxylation on the aliphatic C_{14} of thaxtomin D and aromatic C_{20} of thaxtomin B respectively, while X-ray structure of thaxtomin D complexed in TxtC revealed that it adopts a conformation with its aromatic C_{20} being next to the iron centre of heme, which thus indicates that thaxtomin D could adopt an alternative conformation in the active site of TxtC to fulfil its aliphatic carbon C_{14} hydroxylation. Molecular docking was thus performed to obtain possible binding conformation of thaxtomin D for its C_{14} hydroxylation. The docking results showed that the TxtC-

thaxtomin D complex indeed contains a mixture of two conformations of thaxtomin D. In the docked complex A (see in Figure S1A), thaxtomin D adopts a very similar conformation as that in the X-ray structure(PDB code: 6f0b),[7] while in the second docked complex (complex B, Figure S1B), thaxtomin D lies its aliphatic hydroxylation site C_{14} towards the oxyferryl moiety. Such docking results are in consistence with that were conducted by Challis et al.[7] Further 100 ns MD simulations on the two complexes showed well converged root-mean-squared deviations (RMSDs, as shown in Figure S2), which confirmed that they are both stable binding states. Moreover, MM-PBSA calculations identified that thaxtomin D has very similar binding energy with TxtC in two complexes (−45.3 kcal/mol vs. -44.7 kcal/mol), which further confirmed the speculation that thaxtomin D could adopt two conformations energetically equal in the active site of TxtC. As shown in Figure 1C, in the complex A, the phenyl group of thaxtomin D places over the oxyferryl moiety from the γ-side of the heme. The 4-nitroindole moiety of the substrate, which forms a hydrogen bond with the residue Glu69, is situated in the hydrophobic pocket formed by Leu74, Pro82, Val84, Arg85, Leu228 and Met229. While the L-Phe part of the substrate has hydrophobic contact with the residue Thr385. Compared to that in the complex A, thaxtomin D twists around the C_β–C_γ bond of 4-nitrotryptophan moiety for ~123° in the complex B so that its phenyl group turns to point towards the roof of the active pocket (Figure 1D). Such a conformation allows C_{14} of thaxtomin D to approach the oxyferryl moiety of TxtC in a close distance. In the complex B, the 4-nitrotryptophan group of the substrate stays in the hydrophobic pocket formed by Leu74, Pro82, Val84, Arg85, Leu228 and Met229 as that in the X-ray structure. Such a geometrical layout of complex B ensures reasonable orientation for the observed regiochemistry of aliphatic C_{14} hydroxylation of thaxtomin D. Complex B was then employed to investigate the aliphatic hydroxylation mechanism of thaxtomin D in TxtC.

The aliphatic hydroxylation of thaxtomin D by TxtC

Considering that the active species Cpd I is in the form of triradicaloids[17,18], the sequential tandem hydroxylation processes of thaxtomin D were investigated by two-state reactivity involving doublet (S=1/2) and quartet (S=3/2) spin states by using three different snapshots from MD trajectories as the reactants respectively. Since very similar reaction processes were obtained from these snapshots, here we only discuss one of them, while the rest is provided in the Supporting Information. As displayed in

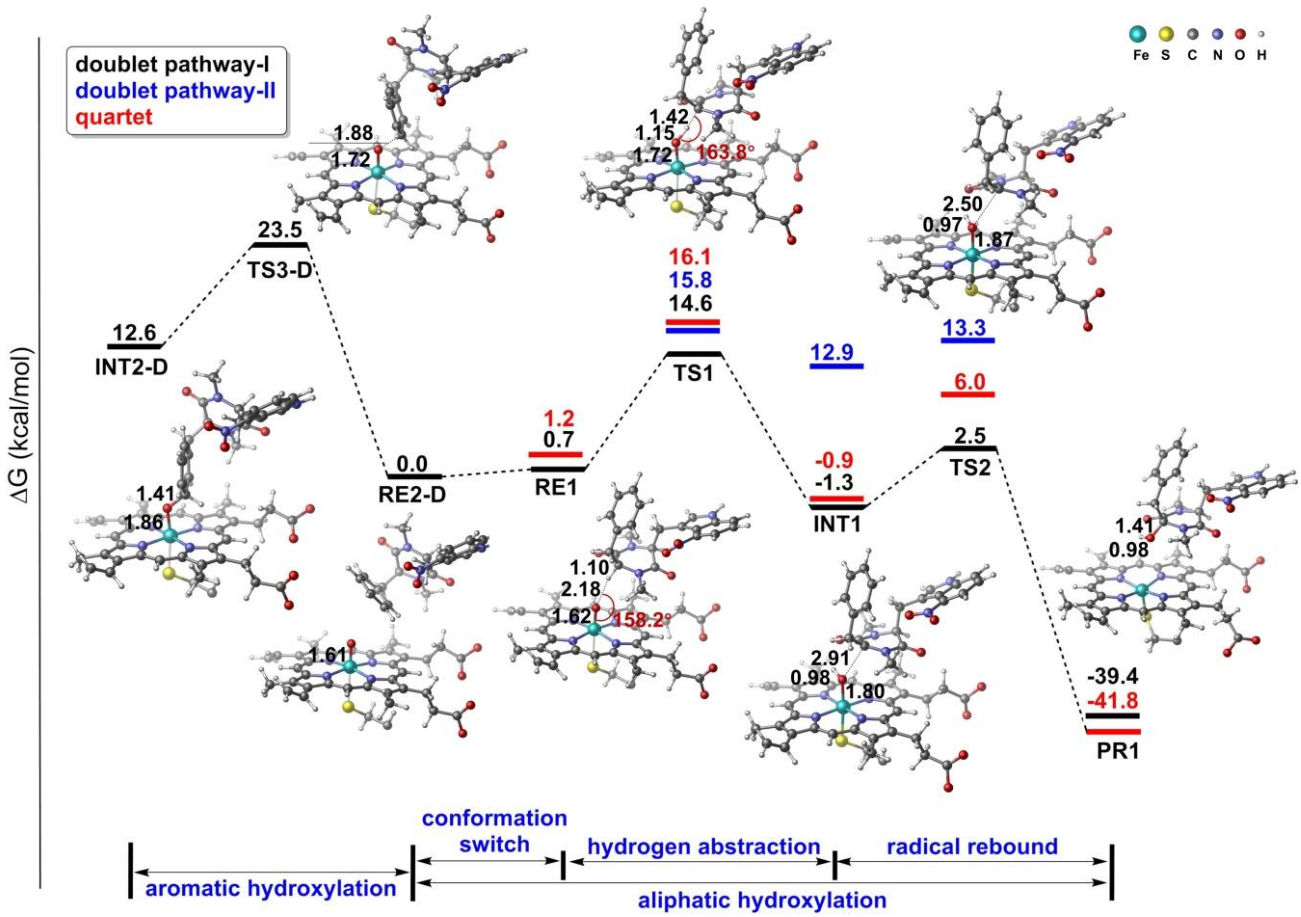

Figure 2 Energy profile of the TxtC-catalysed thaxtomin D aliphatic and aromatic hydroxylation processes. The key structures of the stationary point in the doublet state are shown. Bond lengths are given in Å.

Figure 2, our calculations show that the reaction of C_{14} aliphatic hydroxylation of thaxtomin D proceeds on the doublet state potential energy surface through a rate-limiting hydrogen abstraction step with 14.6 kcal/mol energy barrier, which is followed by a hydroxyl radical rebound step. The following discussion of the thaxtomin D aliphatic hydroxylation reaction in TxtC will be focused on the energetic dominant doublet state.

The thaxtomin D aliphatic hydroxylation process starts from the reactant ^{2}RE1, in which the hydrogen atom on the C_{14} of thaxtomin D points towards the oxyferryl moiety of Cpd I with H···O distance of 2.18 Å and ∠C−H−O of 158.2° (Figure 2). Table 1 displays the spin distribution of the important reaction species during the C_{14} hydroxylation process. Based on the spin population, in ^{2}RE1, two unpaired α electrons reside between oxyferryl moiety, which antiferromagnetically couples with one unpaired β electron residing on the proximal Cys344 ligand. In common Cpd I, the porphyrin ring usually presents as a cationic radical, while in ^{2}RE1, the spin population summed on the porphyrin ring is less than -0.30. Such a spin population indicates that the anionic Cys344 ligand is partially oxidized by the porphyrin moiety in ^{2}RE1.

The conformation of thaxtomin D in ^{2}RE1 allows oxyferryl to selectively abstract hydrogen atom from C_{14} via the transition state ^{2}TS1. In the optimized ^{2}TS1, C_{14}-H-O tends to a collinear arrangement with C_{14}-H bond length and O···H distance of 1.42 Å and 1.15 Å respectively, showing a typical feature of the transition state of C-H bond activation by Fe^{IV}=O species.[43–45] From ^{2}RE1 to ^{2}TS1, along with stretching of the C-H bond, an electron is partially transferred from the substrate to the (Por^+-Cys^-)· moiety, evidenced by the calculated NPA charge on the substrate increasing to +0.41 in ^{2}TS1 (Table S1). The spin population on the substrate decreases to -0.61, while that on (Por^+-Cys^-)· moiety increases to -0.59 from -1.09 in the ^{2}RE1, showing that an electron in α spin is being transferred from the substrate to the Por^+-Cys^- moiety (pathway-I) shown in Scheme S1. It therefore leads us to conclude that this reaction step proceeds via a hydrogen atom transfer (HAT) mechanism. The detailed spin-natural orbitals (SNOs) analysis is demonstrated in Figure S3. This HAT process is the rate-limiting step of the whole C_{14} aliphatic hydroxylation reaction with a 14.6 kcal/mol energy barrier, which generates the transient intermediate ^{2}INT1. ^{2}INT1 is a typical ferryl-hydroxyl species, in which the Fe-O bond length is measured as 1.80 Å. As shown in Table 1, the calculated spin population on the iron and O atoms are 1.84 and 0.21 respectively in ^{2}INT1, corresponding to an intermediate spin state Fe^{IV}-O^{2-}. C_{14} presents as an alkyl radical with spin population on it of -0.62. The following hydroxyl radical rebound step only needs to cross over a very small local barrier of 3.8 kcal/mol and generates TxtC-thaxtomin B complex (P1).

Table 1 The spin population of doublet stationary points in aliphatic hydroxylation of thaxtomin D in TxtC. In this table, the O, Por, sub and H represent oxo moiety of Cpd I, the porphyrin, thaxtomin D and the hydrogen binding on the C_{14}, respectively.

Compound	Fe	O	Cys344	Por	sub	H	C_{14}
RE2	1.33	0.76	-0.79	-0.30	0.01	0.00	0.00
TS1	2.07	0.13	-0.39	-0.20	-0.61	0.02	-0.39
INT1	1.84	0.21	0.07	-0.16	-0.96	0.01	-0.62
TS2	1.62	0.21	0.01	-0.14	-0.71	0.00	-0.45
PR1	1.23	0.00	-0.10	-0.14	0.00	0.00	0.00

Following the similar reaction mechanism, C_{14} hydroxylation reaction could also proceed through another possible mode with β but not α spin electron transferred from the substrate to Cpd I during the HAT process (pathway-II, see in Scheme S1). As shown in Figure 2, the pathway-II is energetically unfavourable than pathway-I. Spin population analysis indicates that this β electron is transferred to the Fe^{IV}=O moiety during HAT. Whereas in the pathway-I, the α electron from substrate goes to the (Por^+-Cys^-)· part, which quenches the (Por^+-Cys^-)· radical thus results in a favourable electron transfer

process in the HAT reaction.

Conformation conversion of thaxtomin B in the active site of TxtC

After C_{14} hydroxylation reaction, to continue hydroxylation on the aromatic C_{20} site, the intermediate thaxtomin B needs to change its conformation to place its aromatic C_{20} site next to the oxyferryl moiety. But whether thaxtomin B accomplishes such conformation switch through releasing-rebinding process or directly flipping over inside the active pocket remains unclear. To investigate how thaxtomin B realizes such conformation switch, MD simulation was performed on the TxtC-thaxtomin B complex in which thaxtomin B adopts the conformation with its hydroxylated C_{14} in close proximity to the heme iron atom which resembles the product state after C_{14} hydroxylation. The TxtC-thaxtomin B complex was then soaked in a TIP3P water box and submitted for 100 ns MD simulation. Interestingly, an obvious interconversion of thaxtomin B from its initial conformation to the one with its phenyl groups laying over the iron center was observed in the MD simulation. The conformation switch of thaxtomin B is characterized by the rotation of L-Phe group around the C_{β}–C_{γ} bond of the 4-nitrotryptophan moiety, which changes significantly during the simulation so that the phenyl group flips to lie over the heme plane (see in Figure 3A). Correspondingly, the energy of the complex system decreases along the simulation (Figure S4). However, such conformational interconversion was not observed in the 100 ns MD simulation of TxtC-thaxtomin D complex (complex B) (Figure 3A). It therefore indicates that the hydroxyl group on the C_{14} is exactly the driving force for the conformation switch of substrate thaxtomin B.

As shown in Figure 3C, in the initial 10 ns MD simulation, Ser280 displays a significant displacement. In initial complex, Ser280 doesn't interact with the substrate but forms a hydrogen bond with Gly366 through the β-hydroxyl (O_{Ser280}-O_{Gly336} = 2.96 Å).At 10 ps, Ser280 has abolished its hydrogen bond interaction with Gly366 but turns to form a new hydrogen bond with the carbonyl group on thaxtomin B. As shown in Figure 3C, this hydrogen bonding interaction pulls the thaxtomin B to deviate from its initial position and further results in that the C_{14}-OH engages in hydrogen bonding interaction with Ser280 (O_{Ser280}-$O_{thaxtomin\ B_hydroxyl}$ distance = 3.25 Å) (11 ps, figure 3C). At 892 ps, Ser280 turns interact with C_{14}-OH exclusively. Through the hydrogen bonding with Ser280, C_{14}-OH group approaches Thr385 at 903 ps. C_{14}-OH turns to hydrogen bond with Thr385 exclusively at 1102 ps. Such a relaying H-bonding interaction between C_{14}-OH and the residues around it lead to that the entire molecule of

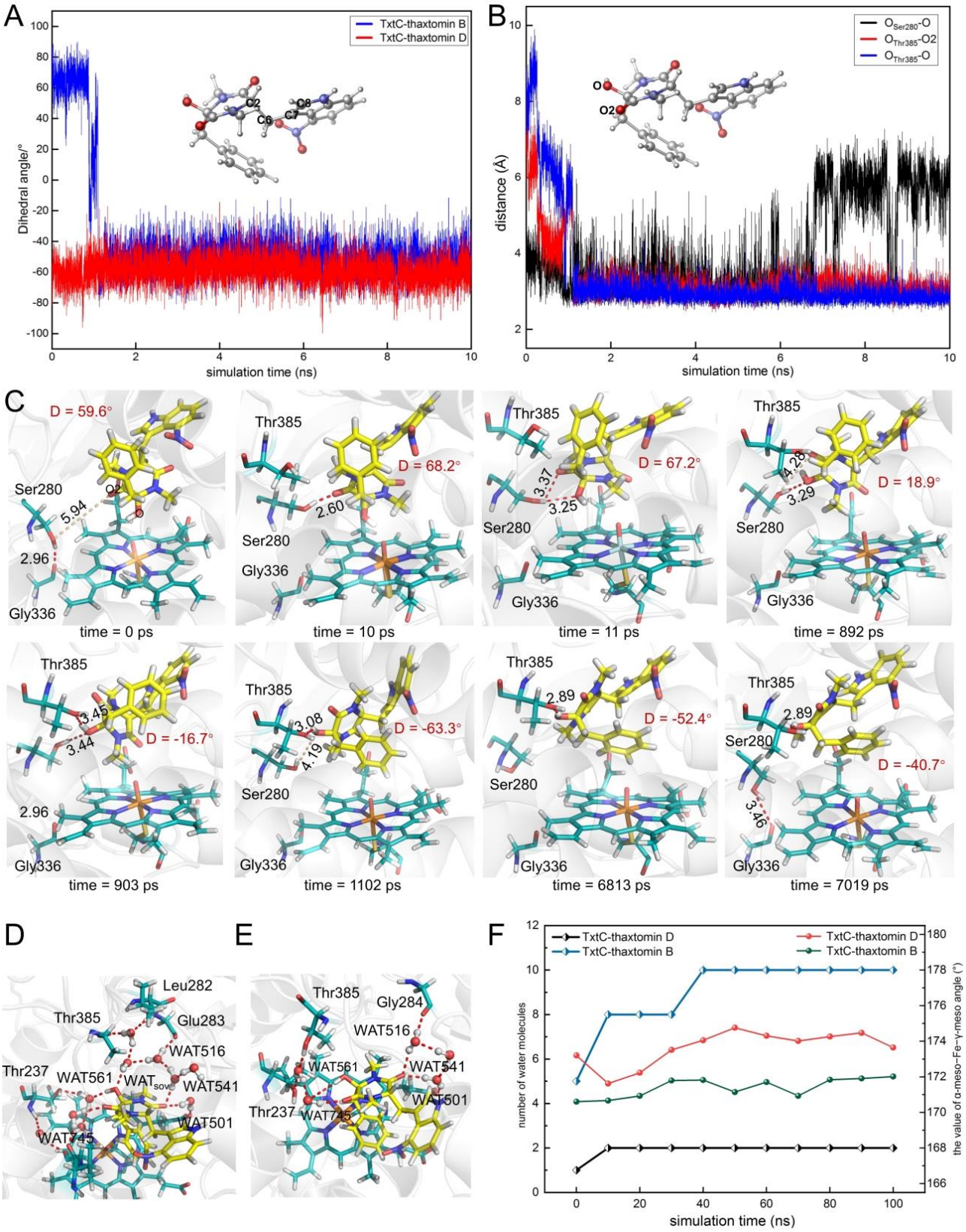

Figure 3 Time-dependences of the C2-C6-C7-C8 dihedral angle variation of thaxtomin B and thaxtomin D (A). The distances variations of the hydrogen bonds between the thaxtomin B and the Ser280 and Thr385 (B) in 10 ns MD simulations. The representative structures in the conformational switch of thaxtomin B from complex B to complex A along the MD simulation (C). TxtC-thaxtomin B in its X-ray structure after 100 ns (D) and 0 ns (E) MD simulations. The quantity of water variation in the binding cavities of thaxtomin D and thaxtomin B were counted with interval setting as 10 ns (F). The key residues in the active site are represented as sticks. Carbon, oxygen, sulfur and nitrogen atoms are coloured in cyan, red, orange and blue respectively. The carbon atoms in the substrate molecules are coloured in yellow. The H-bonds are represented as red dashed lines.

thaxtomin B is lifted away from the heme plane and leaves a space between them, which allows the the L-Phe moiety to rotate around the C_β–C_γ bond of 4-nitrotryptophan and finally switches to the conformation with the phenyl group laying over the heme plane. Such a conformation of thaxtomin B is very similar as that in the X-ray structure of TxtC-thaxtomin B complex. With flipping over of the phenyl group, Ser280 departs away from the C_{14}-OH group, which then gradually returns back to its initial position and restores its hydrogen bonding interaction with Gly336. As a cross-validation, we also performed 100 ns MD simulation on the TxtC-thaxtomin B complex with its initial conformation taken from the X-ray structure (PDB code: 6f0c) in which the phenyl group of thaxtomin B laying on the heme plane already. Interconversion of thaxtomin B is not observed during the simulation (Figure 3D). It therefore leads us to conclude that: 1) thaxtomin D has two equivalent binding conformations in the TxtC's active site. 2) Hydroxylation on the C_{14} site induces conversion of thaxtomin B to reorient its phenyl group toward the oxyferryl moiety. 3) The conformation conversion is irreversible, which enables the second hydroxylation on the aromatic C_{20} site to proceed on a stable binding state of thaxtomin B.

The hydroxyl group on the C_{14} site not only causes conformation conversion of thaxtomin B, it also reshapes the protein environment around it. By comparing the MD simulated complexes of TxtC-thaxtomin D (complex A, from molecular docking) and TxtC-thaxtomin B (X-ray structure, PDB code: 6f0c), one can find some delicate differences between them though the substrate molecules are in very similar orientation in the two complexes. As shown in Figure 3D and Figure S5 in the TxtC-thaxtomin B complex, the polar hydroxyl on C_{14} changes its surrounding environment and induces entrance of water molecules in the active site. An intuitive comparison between two complexes could be found in Figure 3F, in which we plotted the number of the water molecules in the binding cavities of TxtC during 100 ns MD simulations. Figure 3E and 3D depicted two snapshots (0 ns and 100 ns) of TxtC-thaxtomin B complexes during MD simulation which represent the initial and the product structures respectively. One can find that there are two separate hydrogen bond networks formed on the interface between thaxtomin B and TxtC in the initial structure. The one on the left side of Figure 3E is consists two water molecules (WAT561 and 745), residue Thr237 and Thr385, and the carbonyl group of the thaxtomin B. While the carbonyl group of 4-nitrotryptophan moiety, three water molecules (WAT501, 516 and 541), the residue Gly284, and one of the carboxylate side chains on the heme form the other hydrogen bond network in the active site as shown in the right side of Figure 3E. After 100 ns MD

simulation, it can be seen from Figure 3D that these two hydrogen bond networks merged together due to that there are several bulk water molecules joined into them around the hydroxyl group on the C_{14}. Whereas the water molecules presenting in the active site of TxtC-thaxtomin D complex during MD simulation are far less than those in TxtC-thaxtomin B complex. As one can see from Figure S5, for the TxtC-thaxtomin B complex, at the beginning of MD simulation, there is a water molecule (WAT421) in active site which bridges between the 4-nitrotryptophan carbonyl of thaxtomin B and a carboxylate side group of heme. In the 100 ns MD simulation, averagely only one water molecule entered into the active site from the bulk solvent. Such an observation clearly reflects the hydrophobicity of the interface between thaxtomin D and TxtC, which, nevertheless, is changed to hydrophilicity with the hydroxyl group being induced on the C_{14} of thaxtomin B. Though the water molecules induced into the active site by the C_{14}-OH didn't cause any significant tertiary structure change of the protein, they indeed resulted in profound conformation change on the heme plane. These water molecules crowd the active site and force thaxtomin B molecule to move toward the heme ring, of which the phenyl group is pushed to stack on the γ-edge of heme. The steric interaction between the phenyl group of thaxtomin B and the heme ring causes the γ-edge of heme to bend towards the proximal ligand Cys344 and consequently leads to obvious out-of-plane distortion of heme. The angle $C_{\alpha\text{-meso}}$-Fe-$C_{\gamma\text{-meso}}$ could be used to measure the distortion degree of heme plane, during 100 ns simulation, the average angle of $C_{\alpha\text{-meso}}$-Fe-$C_{\gamma\text{-meso}}$ in TxtC-thaxtomin B is 171.5°, which deviates from 180.0° of a planar heme for 8.5°. While thaxtomin D showed less deformation in TxtC with the corresponding $C_{\alpha\text{-meso}}$-Fe-$C_{\gamma\text{-meso}}$ angle of 173.8° during MD simulation. Distortion of the heme could profoundly change the enzyme reactivity even the catalytic mechanism it involved in, which has been well identified in several heme-containing enzymes such as coproheme decarboxylase (ChdC),[46] heme-degrading enzymes from *mycobacterium tuberculosis* (MhuD)[47,48] and *S. aureus* (IsdI).[49]

The aromatic hydroxylation of thaxtomin B by TxtC

Following the MD simulation of TxtC-thaxtomin B, three representative snapshots from MD trajectories were taken for the subsequent ONIOM calculations to investigate the aromatic hydroxylation mechanism of thaxtomin B by TxtC. The most stable spin state for the corresponding reactant (RE2) remains to be the doublet state. In ^{2}RE2, as shown in Figure 4B, thaxtomin B places its phenyl group over the heme ring with the dihedral angle between two molecular planes of ca. 26.4°.

The carbon atom C_{20} of thaxtomin B locates in a distance of 3.51 Å from the γ-meso carbon of heme. The steric interaction between thaxtomin B and heme causes ~1.20 Å of out-of-plane distortion on the

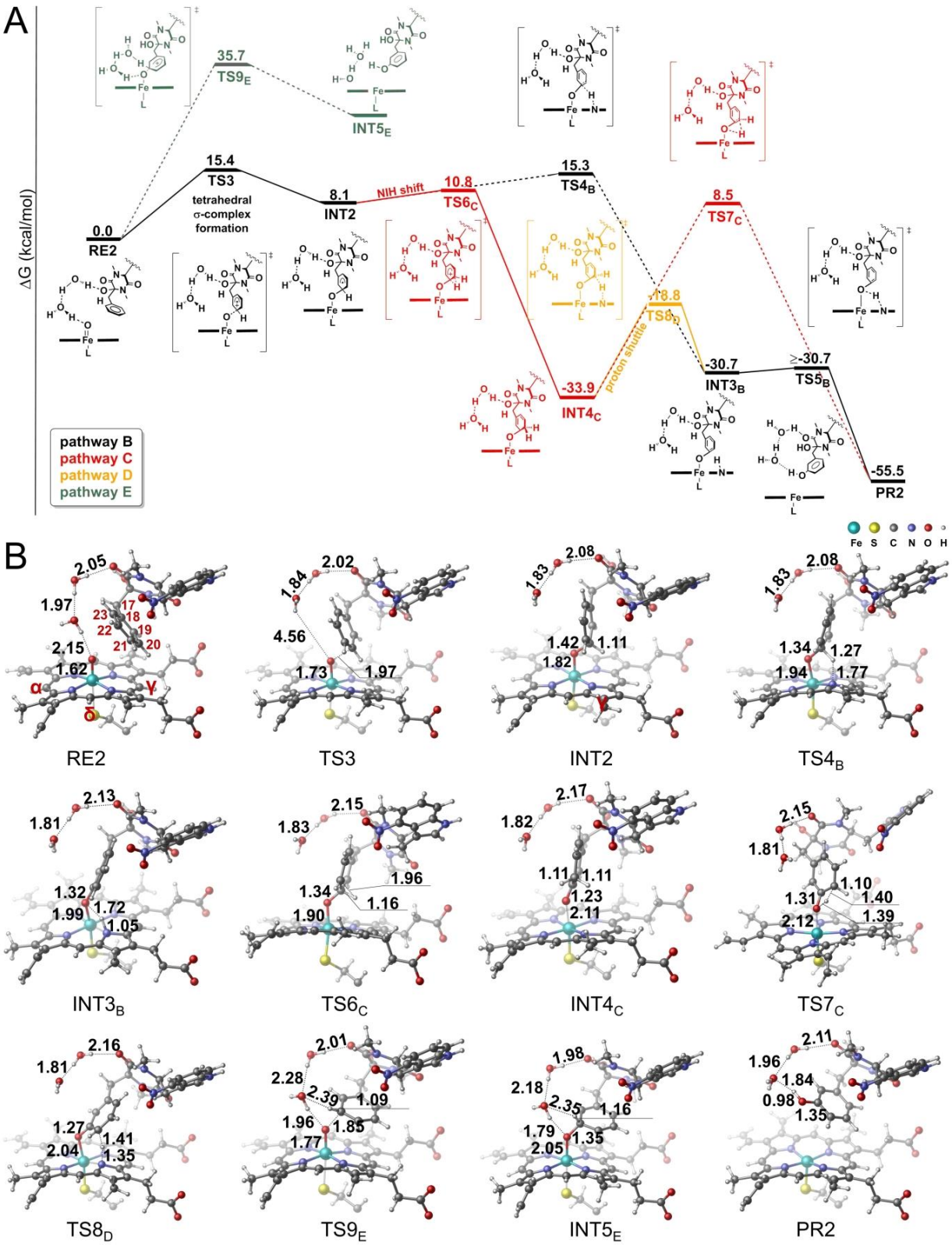

Figure 4 Energy profile of the TxtC-catalysed thaxtomin B aromatic hydroxylation process in doublet state (A). Some key structures of the stationary points along the aromatic hydroxylation in the doublet state of in TxtC are shown (B). Bond lengths are given in Å.

heme plane (measured by Normal Coordinate Structural Decomposition (NSD)).[47,50]

Following the Pathway B as shown in Scheme 1, from ^{2}RE2, the first step of aromatic hydroxylation of thaxtomin B is addition of the phenyl group to the iron-oxo moiety, which proceeds on the doublet state potential energy surface by crossing over a transition state (^{2}TS3) with 15.4 kcal/mol energy barrier (see in Figure 4A) (By using the other two snapshots as the initial structures of the reactant, 16.7 kcal/mol and 16.8 kcal/mol energy barrier were obtained). The optimized geometry structure of ^{2}TS3 shows that the phenyl group of thaxtomin B rotates for 4.5° around the C17-C18 from that in ^{2}RE2, so that the oxo places close to the C_{20} within a distance of 1.97 Å. In the ^{2}TS3, the C_{20} protrudes out the phenyl plane to approach the oxyferryl moiety, meanwhile the Fe-O bond stretches to 1.73 Å. In the ^{2}TS3, the phenyl group of thaxtomin D displays a mixed cationic and radical character. At the ^{2}TS3 stage, an electron from the substrate has been partially transferred to the Cpd I moiety, as evidenced by the +0.31 charge carried by the phenyl group of thaxtomin B. The electron transfer process from ^{2}RE2 to ^{2}TS3 could also be visualized from their electrostatic potential diagrams depicted in Figure S6.

By crossing over ^{2}TS3, C_{20}-O bond forms and generates the tetrahedral σ-complex intermediate ^{2}INT2, which is endothermic for 8.1 kcal/mol. In the σ-complex intermediate ^{2}INT2, C_{20} converts to sp^3 hybridization with C_{20}-H folding out of the phenyl plane towards the γ-meso carbon of heme. The two C-C bonds of C_{20} with its adjacent carbon (C_{20}-C_{21} and C_{19}-C_{20}) on the phenyl group both extend to 1.50 Å in ^{2}INT2 (see in Table S4). The next step is heterolysis of C_{20}-H of which the proton is transferred to one of the pyrrole nitrogen atoms of the porphyrin to produce a N-protonated porphyrin complex (^{2}INT3$_B$), which goes through the transition state ^{2}TS4$_B$ with 7.2 kcal/mol local energy barrier (Figure 4A). The geometry structure of ^{2}INT3$_B$ is shown in Figure 4B, one can find that protonation of the pyrrole nitrogen causes severe buckling to the porphyrin, so that the corresponding pyrrole fragment flips out from the porphyrin plane. From ^{2}INT3$_B$, the proton on the pyrrole nitrogen could feasibly shuttle to the negative charged oxygen atom of oxyferryl moiety in vicinity, which results in Fe-O bond fully cleavage and produces thaxtomin A. This last transformation step takes place on a very flat area of the potential energy surface, so that the reaction step is almost barrierless. It is very similar as the benzene hydroxylation process catalyzed by cytochrome P450 which has been reported in a previous study.[20]

Table 2 Calculated Mulliken Spin population on various moieties in aromatic hydroxylation of thaxtomin B. In this table, the O, Por, sub, N and H represent oxo moiety of Cpd I, the porphyrin, thaxtomin B, the pyrrole nitrogen atoms of the porphyrin and the hydrogen binding on the C_{20}, respectively.

Compound	Por	Cys	sub	Fe	O	N	H
RE2	-0.27	-0.82	0.00	1.31	0.78	-0.10	0.00
TS3	-0.19	-0.06	-0.40	1.76	-0.12	-0.05	-0.01
INT2	-0.14	0.06	-0.91	1.81	0.17	-0.04	-0.03
$TS4_B$	-0.08	0.12	0.00	0.95	0.02	-0.01	0.00
$INT3_B$	-0.08	0.12	0.01	0.91	0.02	-0.01	0.00
$TS6_C$	-0.09	0.13	-0.16	1.06	0.05	-0.02	0.00
$INT4_C$	-0.08	0.09	0.00	0.98	0.00	-0.02	0.00
$TS7_C$	-0.07	0.12	0.00	0.95	0.00	-0.02	0.00
$TS8_D$	-0.08	0.12	0.00	0.95	0.00	-0.02	0.00
$TS9_E$	-0.14	-0.88	0.31	1.15	0.55	-0.01	0.00
PR2	-0.09	0.02	0.00	1.07	0.00	-0.02	0.00

From the tetrahedral σ-complex intermediate ^{2}INT2, proton immigration from C_{20} to O atom could proceed through an alternative pathway which is mediated by the para-carbon C21 of the phenyl group (NIH shift). This NIH shift process experiences an early stage transition state $^2TS6_C$ which closely resembles ^{2}INT2 with a very low local barrier of 2.7 kcal/mol, in which the C_{20}-H bond only stretches for 0.05 Å from that in ^{2}INT2. After crossing the proton immigration transition state $^2TS6_C$, the resulted intermediate $^2INT4_C$ drops dramatically in energy for 42.0 kcal/mol from ^{2}INT2. Such an exothermic process from ^{2}INT2 to $^2INT4_C$ could be rationalized by the fact that the phenyl group of substrate in ^{2}INT2 is in the form of a radical cation, as evidenced by net -0.91 spin population on it, which is quenched with the C21-H bond formation in $^2INT4_C$, corresponding to a β electron transferred from the phenyl group to the oxyferryl moiety. In $^2INT4_C$, the C_{20}-C_{21} bond stretches to 1.51 Å, while C_{20}-C_{19} restores to 1.45 Å (see in Table S4). From $^2INT4_C$, the proton shifts from C21 to the O and produces the final product thaxtomin A. The proton shifting process could either proceed directly (pathway C) or mediated by the pyrrole nitrogen from the porphyrin ring (pathway D). Our calculations show that pathway C needs to cross over a very high energy barrier of 42.4 kcal/mol, due to the severe steric tension of the rhombic shape proton transfer transition structure ($^2TS7_C$, Figure 4). While pathway D is the dominant one within which the reaction experiences the transition state $^2TS8_D$ with energy barrier of 15.1 kcal/mol and generates $^2INT5_B$ to merge in the pathway B. It is worth to note that this three stages pathway which consists of tetrahedral σ-complex intermediate (INT2) formation, NIH shift and proton shuttle bypasses the energetic unfavorable proton shift transition state $^2TS4_B$ via protonation of pyrrole nitrogen of the prophyrin, which therefore becomes the most favorable mechanism for the

aromatic hydroxylation of thaxtomin B in TxtC.

Heme distortion in TxtC

As discussed above, we have explored the catalytic mechanisms of aliphatic hydroxylation of thaxtomin D and aromatic hydroxylation of thaxtomin B in TxtC. The calculation results indicated that the rate-limiting step of aromatic hydroxylation on thaxtomin B experiences slighter higher energy barrier than that of the aliphatic hydroxylation of thaxtomin D (15.4 kcal/mol vs. 14.6 kcal/mol). However, previous kinetic experiment determined that the catalytic efficiency of TxtC in aliphatic carbon hydroxylation is in the same order of aromatic hydroxylation with corresponding energy barrier in the rate-limiting step of ~14.8 kcal/mol and ~15.0 kcal/mol, respectively.[3] Thus the calculation results still don't explain why TxtC displays the observed regioselectivtity to preferentially hydroxylation on the aliphatic C_{14} of thaxtomin D.

To elucidate the regioselectivity of TxtC to preferentially hydroxylate on the aliphatic C_{14} of thaxtomin D, we further investigated the aromatic hydroxylation process of thaxtomin D in TxtC with ONIOM calculations. The docked structure of complex A of TxtC-thaxtomin D after MD simulation was employed to build the initial reactant (RE2-D) and submitted for geometry optimization. An obvious structural character of ^{2}RE2-D which is different from ^{2}RE2 (the aromatic hydroxylation reactant of thaxtomin B in TxtC) is that the heme ring in it maintains in a planar conformation. The measured NSD out-of-plane degree of heme in RE2-D is only 0.34 Å. Based on RE2-D, we investigated the aromatic hydroxylation process of thaxtomin D. It is interesting to find that the calculated energy barrier of the rate-limiting step to generate the tetrahedral σ-complex intermediate increases to 23.5 kcal/mol, which clearly suggests that without the hydroxyl group on the C_{14}, aromatic hydroxylation of thaxtomin D would be much slower. This calculation result also rationalizes the observed regioselectivity of TxtC to preferentially hydroxylate on the aliphatic C_{14} site of thaxtomin D. A plausible explanation for the higher reactivity of thaxtomin B on its aromatic site after hydroxylation on C_{14} could be ascribed to larger distortion of the heme in RE2 (NSD: 1.20 Å) than that in RE2-D (NSD: 0.34 Å). Our MD simulation have revealed that the hydroxyl substituent on C_{14} induces several bulk water molecules to enter into the active pocket, which push thaxtomin B toward the heme plane and cause considerable distortion on it. With that in mind, we manually removed the water molecules which are induced into the active pocket by the hydroxyl group on the C_{14} site and performed

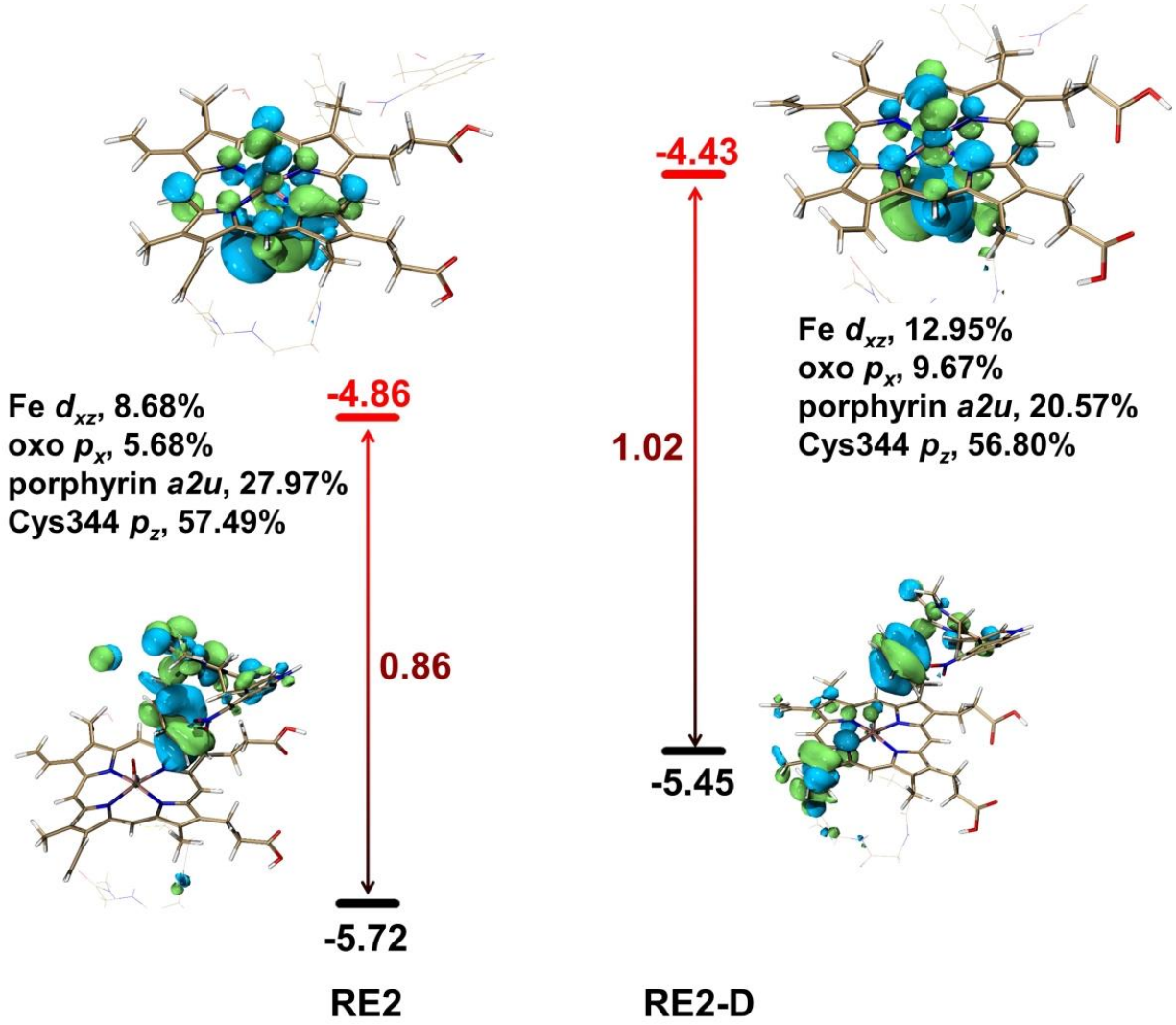

Figure 5 The highest occupied α-orbital of two substrates (black line) and the lowest α-vacant orbital of Cpd I (red line) with their energies (in eV) for ^{2}RE2 and ^{2}RE2-D in the doublet state. The main compositions of the lowest α-vacant orbital of Cpd I also are depicted (%).

calculation on the rate-limiting tetrahedral σ-complex formation step on the TxtC-thaxtomin B complex again. As shown in Figure S7, without water molecules accumulating around C_{14} and pushing thaxtomin B to the heme plane, the heme ring restores to a planar shape with overall out-of-plane distortions degree descending to 0.66 Å after optimization. Correspondingly, the calculated energy barrier increases to 22.9 kcal/mol. Further computational studies were performed on a control model in which the water molecules around C_{14} were removed while the heme ring is restrained in a distortion conformation as that in RE2, with which the energy barrier of the rate-limiting step is calculated to be 15.5 kcal/mol. Therefore, these calculations clearly revealed the fact that the hydroxyl group on C_{14} of thaxtomin B promotes the reactivity of its aromatic hydroxylation by causing distortion of the heme plane.

Since our calculation results revealed that aromatic hydroxylation of thaxtomin B is rate-limited by

the tetrahedral σ-complex formation step in which an α electron is transferred from the phenyl group of the substrate to Cpd I. To investigate why the out-of-plane distortion of heme promotes the reactivity of aromatic hydroxylation of thaxtomin B in this step, it is intuitive to look into the frontier orbitals (FMO) of the reactant complex. In the Figure 5, we depicted the lowest vacant α-orbital of RE2-D. It presents as an anti-bonding molecular orbital which consists of the components of the a2u fragment orbital from the porphyrin ring, the d_{xz} orbital from the iron center and the p_x orbital from the sulfur atom of the Cys344 ligand. The calculated energy level of this orbital is -4.43 eV, which is 1.02 eV higher than the highest occupied α-orbital of thaxtomin D that populates on the phenyl group. While in ^{2}RE2, the energy level of the lowest vacant α-orbital decreases to -4.86 eV, despite that the highest occupied α-orbital of thaxtomin B also decreases to 0.27 eV due to the hydroxyl substitution on its C_{14} site, the energy gap still decreases to 0.86 eV. Obviously, such a narrower energy gap of ^{2}RE2 is consistent with its lower energy barrier to reach the tetrahedral σ-complex formation transition state. By analyzing the orbital components of their FMO (Figure 5), one can find that the proportions of the fragment orbitals from the porphyrin, the iron center and the sulfur atom of Cys344 ligand are changed from RE2-D to RE2 due to the out-of-plane distortion of heme. Especially, the distortion of heme decreases the anti-bonding overlap between the a2u orbital from porphyrin and d_{xz} of the iron center, which therefore results in a lower energy level of this anti-bonding orbital. Similar orbital composition change caused by heme out-of-plane distortion has also observed in some heme-containing enzymes such as *coproheme decarboxylase* (ChdC), heme-degrading enzymes from *mycobacterium tuberculosis* (MhuD) and *S. aureus* (IsdI). Based on the FMO analysis of RE2 and RE2-D, we come to a conclusion that the out-of-plane distortion of heme, which is caused by the hydrogen bond interaction between the thaxtomin B and the surrounding water molecules induced by C_{14} hydroxyl group, is crucial for the aromatic hydroxylation of substrate by enhancing the electrophilicity of Cpd I.

CONCLUSIONS

In this work, molecule docking and MD simulation showed that thaxtomin D is able to adopt a mixture of two conformations in the active site of TxtC, in which either its aromatic C_{20}-H or aliphatic C_{14}-H laying towards the active oxyferryl moiety of Cpd I. The sequential aliphatic and aromatic hydroxylation mechanisms of thaxtomin D by TxtC were then investigated by

using ONIOM calculations in detail. Calculation results revealed that the aliphatic hydroxylation on C_{14} site of thaxtomin D is 8.9 kcal/mol energetically favourable than its aromatic hydroxylation, which is in consistence with the experimental observed regioselectivity of TxtC to hydroxylate on the aliphatic C_{14} site of thaxtomin D. MD simulation on the complex of TxtC with C_{14} hydroxylated intermediate thaxtomin B revealed that the hydroxyl group on C_{14} site plays a crucial role to promote the substrate to flip over by placing the aromatic C-H next to the oxyferryl centre. The C_{14}-OH group also induces the bulk water to enter into the active site so that the substrate thaxtomin B is pushed towards the heme and results in the distortion of the heme plane, which finally accelerate the aromatic hydroxylation reaction by enhancing the electrophilicity of Cpd I.

CONFLICTS OF INTEREST

"There are no conflicts to declare".

ACKNOWLEDGEMENTS

This work was supported by grants from the National Key Research and Development Program of China (no. 2019YFC1805600) and the National Natural Science Foundation of China (no. 21571019, 21573020 and 21503018).

(1) Fry, B. A.; Loria, R. Thaxtomin A: Evidence for a Plant Cell Wall Target. *Physiol. Mol. Plant Pathol.* **2002**, *60*, 1–8.

(2) Loria, R.; Bignell, D. R. D.; Moll, S.; Huguet-Tapia, J. C.; Joshi, M. V.; Johnson, E. G.; Seipke, R. F.; Gibson, D. M. Thaxtomin Biosynthesis: The Path to Plant Pathogenicity in the Genus Streptomyces. *Antonie van Leeuwenhoek, Int. J. Gen. Mol. Microbiol.* **2008**, *94*, 3–10.

(3) Jiang, G.; Zuo, R.; Zhang, Y.; Powell, M. M.; Zhang, P.; Hylton, S. M.; Loria, R.; Ding, Y. One-Pot Biocombinatorial Synthesis of Herbicidal Thaxtomins. *ACS Catal.* **2018**, *8*, 10761–10768.

(4) Jiang, G.; Zhang, Y.; Powell, M. M.; Hylton, S. M.; Hiller, N. W.; Loria, R.; Ding, Y. A Promiscuous Cytochrome P450 Hydroxylates Aliphatic and Aromatic C−H Bonds of Aromatic 2,5-Diketopiperazines. *ChemBioChem* **2019**, *20*, 1068–1077.

(5) Zhang, H.; Ning, X.; Hang, H.; Ru, X.; Li, H.; Li, Y.; Wang, L.; Zhang, X.; Yu, S.; Qiao, Y.; Wang,

X.; Wang, P. G. Total Synthesis of Thaxtomin A and Its Stereoisomers and Findings of Their Biological Activities. *Org. Lett.* **2013**, *15*, 5670–5673.

(6) Balalaie, S.; Ramezani Kejani, R.; Ghabraie, E.; Darvish, F.; Rominger, F.; Hamdan, F.; Bijanzadeh, H. R. Diastereoselective Synthesis of Functionalized Diketopiperazines through Post-Transformational Reactions. *J. Org. Chem.* **2017**, *82*, 12141–12152.

(7) Alkhalaf, L. M.; Barry, S. M.; Rea, D.; Gallo, A.; Griffiths, D.; Lewandowski, J. R.; Fulop, V.; Challis, G. L. Binding of Distinct Substrate Conformations Enables Hydroxylation of Remote Sites in Thaxtomin D by Cytochrome P450 TxtC. *J. Am. Chem. Soc.* **2019**, *141*, 216–222.

(8) Haslinger, K.; Peschke, M.; Brieke, C.; Maximowitsch, E.; Cryle, M. J. X-Domain of Peptide Synthetases Recruits Oxygenases Crucial for Glycopeptide Biosynthesis. *Nature* **2015**, *521*, 105–109.

(9) Barry, S. M.; Kers, J. A.; Johnson, E. G.; Song, L.; Aston, P. R.; Patel, B.; Krasnoff, S. B.; Crane, B. R.; Gibson, D. M.; Loria, R.; Challis, G. L. Cytochrome P450-Catalyzed L-Tryptophan Nitration in Thaxtomin Phytotoxin Biosynthesis. *Nat. Chem. Biol.* **2012**, *8*, 814–816.

(10) Podust, L. M.; Sherman, D. H. Diversity of P450 Enzymes in the Biosynthesis of Natural Products. *Nat. Prod. Rep.* **2012**, *29*, 1251–1266.

(11) Song, L.; Laureti, L.; Corre, C.; Leblond, P.; Aigle, B.; Challis, G. L. Cytochrome P450-Mediated Hydroxylation Is Required for Polyketide Macrolactonization in Stambomycin Biosynthesis. *J. Antibiot. (Tokyo).* **2014**, *67*, 71–76.

(12) Zabala, D.; Cartwright, J. W.; Roberts, D. M.; Law, B. J. C.; Song, L.; Samborskyy, M.; Leadlay, P. F.; Micklefield, J.; Challis, G. L. A Flavin-Dependent Decarboxylase-Dehydrogenase-Monooxygenase Assembles the Warhead of α,β-Epoxyketone Proteasome Inhibitors. *J. Am. Chem. Soc.* **2016**, *138*, 4342–4345.

(13) Li, D.; Wang, Y.; Han, K. Recent Density Functional Theory Model Calculations of Drug Metabolism by Cytochrome P450. *Coord. Chem. Rev.* **2012**, *256*, 1137–1150.

(14) Kamachi, T.; Yoshizawa, K. A Theoretical Study on the Mechanism of Camphor Hydroxylation by Compound I of Cytochrome P450. *J. Am. Chem. Soc.* **2003**, *125*, 4652–4661.

(15) De Visser, S. P.; Kumar, D.; Cohen, S.; Shacham, R.; Shaik, S. A Predictive Pattern of Computed Barriers for C-H Hydroxylation by Compound I of Cytochrome P450. *J. Am. Chem. Soc.* **2004**, *126*, 8362–8363.

(16) Shaik, S.; Kumar, D.; de Visser, S. P.; Altun, A.; Thiel, W. *Theoretical Perspective on the Structure*

and Mechanism of Cytochrome P450 Enzymes; 2005; Vol. 105.

(17) Shaik, S.; Cohen, S.; Wang, Y.; Chen, H.; Kumar, D.; Thiel, W. P450 Enzymes: Their Structure, Reactivity, and Selectivity - Modeled by QM/MM Calculations. *Chem. Rev.* **2010**, *110*, 949–1017.

(18) Meunier, B.; de Visser, S. P.; Shaik, S. Mechanism of Oxidation Reactions Catalyzed by Cytochrome P450 Enzymes. *Chem. Rev.* **2004**, *104*, 3947–3980.

(19) Bathelt, C. M.; Mulholland, A. J.; Harvey, J. N. QM/MM Modeling of Benzene Hydroxylation in Human Cytochrome P450 2C9. *J. Phys. Chem. A* **2008**, *112*, 13149–13156.

(20) De Visser, S. P.; Shaik, S. A Proton-Shuttle Mechanism Mediated by the Porphyrin in Benzene Hydroxylation by Cytochrome P450 Enzymes. *J. Am. Chem. Soc.* **2003**, *125*, 7413–7424.

(21) Sono, M.; Roach, M. P.; Coulter, E. D.; Dawson, J. H. Heme-Containing Oxygenases. *Chem. Rev.* **1996**, *96*, 2841–2887.

(22) Korzekwa, K. R.; Swinney, D. C.; Trager, W. F. Isotopically Labeled Chlorobenzenes as Probes for the Mechanism of Cytochrome P-450 Catalyzed Aromatic Hydroxylation. *Biochemistry* **1989**, *28*, 9019–9027.

(23) Li, X. X.; Wang, Y.; Zheng, Q. C.; Zhang, H. X. Detoxification of 1-Methyl-4-Phenyl-1,2,3,6-Tetrahydropyridine (MPTP) by Cytochrome P450 Enzymes: A Theoretical Investigation. *J. Inorg. Biochem.* **2016**, *154*, 21–28.

(24) Woon, J. S.; Yon, O. R.; Song, R.; Nam, W. Oxoiron(IV) Porphyrin π-Cation Radical Complexes with a Chameleon Behavior in Cytochrome P450 Model Reactions. *J. Biol. Inorg. Chem.* **2005**, *10*, 294–304.

(25) De Visser, S. P.; Tahsini, L.; Nam, W. How Does the Axial Ligand of Cytochrome P450 Biomimetics Influence the Regioselectivity of Aliphatic versus Aromatic Hydroxylation? *Chem. - A Eur. J.* **2009**, *15*, 5577–5587.

(26) De Visser, S. P.; Ogliaro, F.; Sharma, P. K.; Shaik, S. What Factors Affect the Regioselectivity of Oxidation by Cytochrome P450? A DFT Study of Allylic Hydroxylation and Double Bond Epoxidation in a Model Reaction. *J. Am. Chem. Soc.* **2002**, *124*, 11809–11826.

(27) Allouche, A. Software News and Updates Gabedit — A Graphical User Interface for Computational Chemistry Softwares. *J. Comput. Chem.* **2009**, *30*, 2785–2791.

(28) Docking, A. J. A.; Autodock, A. J. Zusammenfassung Verschiedener AutoDock Paper. *J. Comput. Chem.* **1998**, *19*, 1639–1662.

(29) Dolinsky, T. J.; Nielsen, J. E.; McCammon, J. A.; Baker, N. A. PDB2PQR: An Automated Pipeline for the Setup of Poisson-Boltzmann Electrostatics Calculations. *Nucleic Acids Res.* **2004**, *32*, 665–667.

(30) Maier, J. A.; Martinez, C.; Kasavajhala, K.; Wickstrom, L.; Hauser, K. E.; Simmerling, C. Ff14SB: Improving the Accuracy of Protein Side Chain and Backbone Parameters from Ff99SB. *J. Chem. Theory Comput.* **2015**, *11*, 3696–3713.

(31) Wang, J.; Wolf, R. M.; Caldwell, J. W.; Kollman, P. A.; Case, D. A. Development and Testing of a General Amber Force Field. *J. Comput. Chem.* **2004**, *25*, 1157–1174.

(32) Wang, J.; Wang, W.; Kollman, P. A.; Case, D. A. Automatic Atom Type and Bond Type Perception in Molecular Mechanical Calculations. *J. Mol. Graph. Model.* **2006**, *25*, 247–260.

(33) Shahrokh, K.; Orendt, A.; Yost, G. S.; Cheatham, T. E. Quantum Mechanically Derived AMBER-Compatible Heme Parameters for Various States of the Cytochrome P450 Catalytic Cycle. *J. Comput. Chem.* **2012**, *33*, 119–133.

(34) Jorgensen, W. L.; Chandrasekhar, J.; Madura, J. D.; Impey, R. W.; Klein, M. L. Comparison of Simple Potential Functions for Simulating Liquid Water. *J. Chem. Phys.* **1983**, *79*, 926–935.

(35) Dapprich, S.; Komáromi, I.; Byun, K. S.; Morokuma, K.; Frisch, M. J. A New ONIOM Implementation in Gaussian98. Part I. The Calculation of Energies, Gradients, Vibrational Frequencies and Electric Field Derivatives. *J. Mol. Struct. THEOCHEM* **1999**, *461–462*, 1–21.

(36) Tao, P.; Schlegel, H. B. Software News and Updates A Toolkit to Assist ONIOM Calculations. *J. Comput. Chem.* **2010**, *31*, 2363–2369.

(37) Becke, A. D. Density-Functional Thermochemistry. III. The Role of Exact Exchange. *J. Chem. Phys.* **1993**, *98*, 5648–5652.

(38) Schäfer, A.; Horn, H.; Ahlrichs, R. Fully Optimized Contracted Gaussian Basis Sets for Atoms Li to Kr. *J. Chem. Phys.* **1992**, *97*, 2571–2577.

(39) Cornell, W. D.; Cieplak, P.; Bayly, C. I.; Gould, I. R.; Merz, K. M.; Ferguson, D. M.; Spellmeyer, D. C.; Fox, T.; Caldwell, J. W.; Kollman, P. A. A Second Generation Force Field for the Simulation of Proteins, Nucleic Acids, and Organic Molecules. *J. Am. Chem. Soc.* **1995**, *117*, 5179–5197.

(40) Frisch, M. J.; Trucks, G. W.; Schlegel, H. B.; Scuseria, G. E.; Robb, M. A.; Cheeseman, J. R.; Scalmani, G.; Barone, V.; Mennucci, B.; Petersson, G. A.; Nakatsuji, H.; Caricato, M.; Li, X.; Hratchian, H. P.; Izmaylov, A. F.; Bloino, J.; Zheng, G.; Sonnenb.

(41) Grimme , J. Antony, S. E. and H. K. Parametrization of Density Functional Dispersion Correction

(DFT-D) for the 94 Elements H-Pu Dispersion Correction „ DFT-D … for the 94 Elements H-Pu. *J. Chem. Phys.* **2010**, *132*.

(42) Pritchard, B. P.; Altarawy, D.; Didier, B.; Gibson, T. D.; Windus, T. L. New Basis Set Exchange: An Open, Up-to-Date Resource for the Molecular Sciences Community. *J. Chem. Inf. Model.* **2019**, *59*, 4814–4820.

(43) Yoshizawa, K.; Shiota, Y.; Yamabe, T. Abstraction of the Hydrogen Atom of Methane by Iron-Oxo Species: The Concerted Reaction Path Is Energetically More Favorable. *Organometallics* **1998**, *17*, 2825–2831.

(44) Yumura, T.; Yoshizawa, K. Regioselectivity in 2-Methylbutane Hydroxylation Mediated by FeO+ and FeO2+. *Organometallics* **2001**, *20*, 1397–1407.

(45) Ohta, T.; Kamachi, T.; Shiota, Y.; Yoshizawa, K. A Theoretical Study of Alcohol Oxidation by Ferrate. *J. Org. Chem.* **2001**, *66*, 4122–4131.

(46) Zhang, Y.; Wang, J.; Yuan, C.; Liu, W.; Tan, H.; Li, X.; Chen, G. Ruffling Drives Coproheme Decarboxylation by Facilitating PCET: A Theoretical Investigation of ChdC. *Phys. Chem. Chem. Phys.* **2020**, *22*, 16117–16124.

(47) Graves, A. B.; Graves, M. T.; Liptak, M. D. Measurement of Heme Ruffling Changes in MhuD Using UV-Vis Spectroscopy. *J. Phys. Chem. B* **2016**, *120*, 3844–3853.

(48) Graves, A. B.; Horak, E. H.; Liptak, M. D. Dynamic Ruffling Distortion of the Heme Substrate in Non-Canonical Heme Oxygenase Enzymes. *Dalt. Trans.* **2016**, *45*, 10058–10067.

(49) Woo, C. L.; Reniere, M. L.; Skaar, E. P.; Murphy, M. E. P. Ruffling of Metalloporphyrins Bound to IsdG and IsdI, Two Heme-Degrading Enzymes in Staphylococcus Aureus. *J. Biol. Chem.* **2008**, *283*, 30957–30963.

(50) Jentzen, W.; Song, X. Z.; Shelnutt, J. A. Structural Characterization of Synthetic and Protein-Bound Porphyrins in Terms of the Lowest-Frequency Normal Coordinates of the Macrocycle. *J. Phys. Chem. B* **1997**, *101*, 1684–1699.

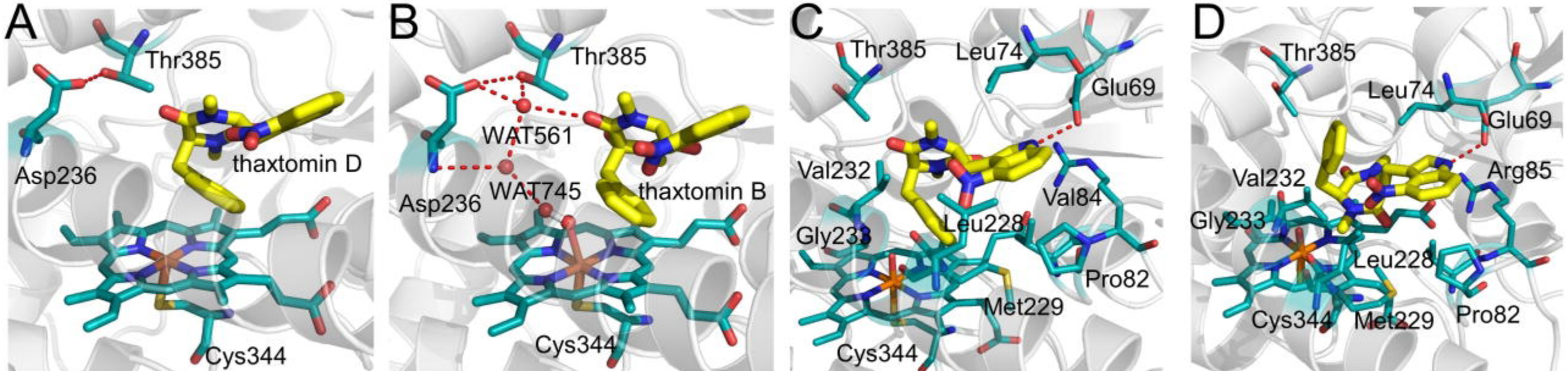
A
Thr385
Asp236
thaxtomin D
Cys344
B
Thr385
WAT561
Asp236
WAT745
thaxtomin B
Cys344
C
Thr385
Leu74
Glu69
Val232
Val84
Leu228
Gly233
Pro82
Met229
Cys344
D
Thr385
Leu74
Glu69
Arg85
Val232
Gly233
Leu228
Cys344
Met229
Pro82

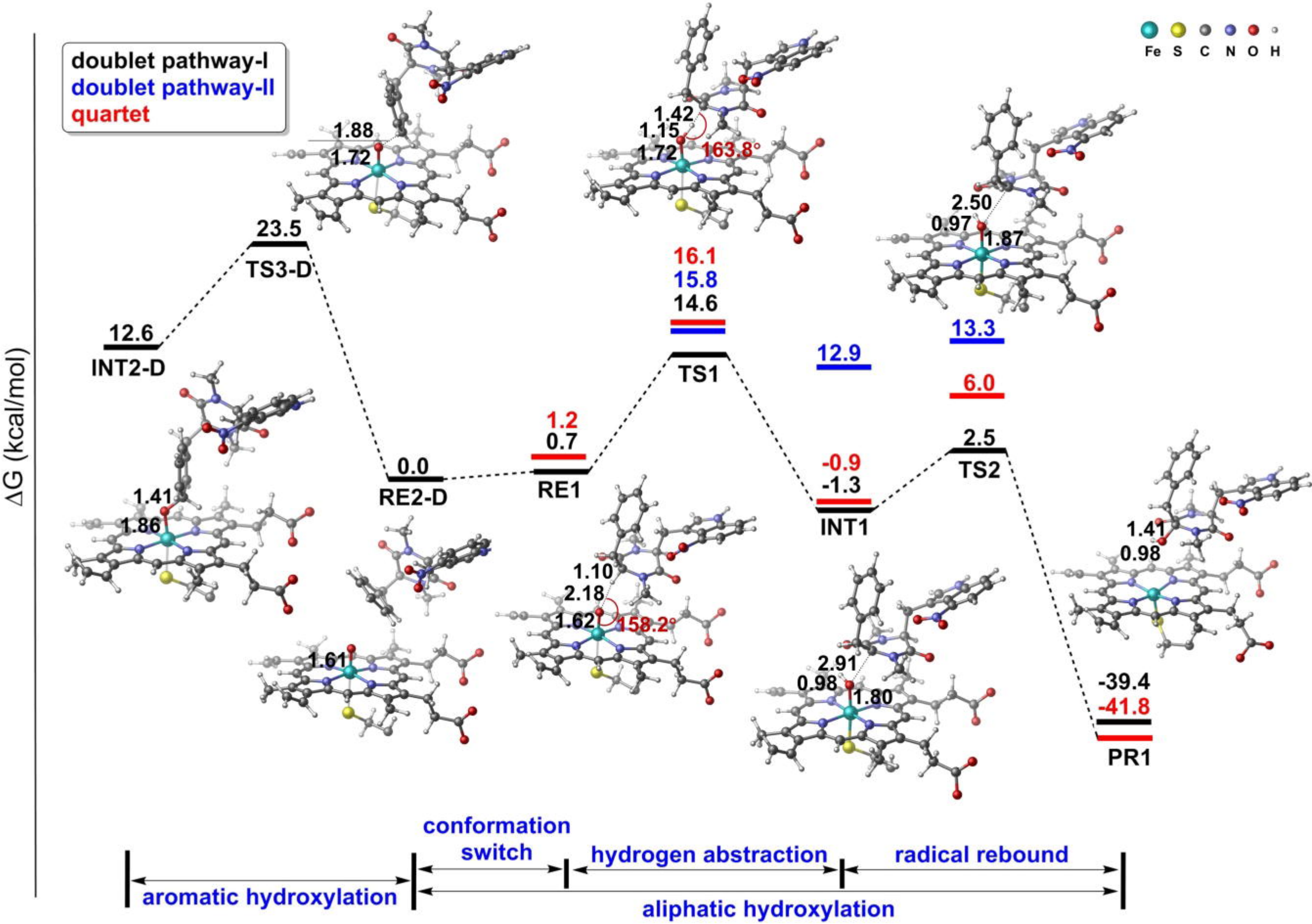
doublet pathway-I
doublet pathway-II
quartet
Fe S C N O H
ΔG (kcal/mol)
1.88
1.72
23.5
TS3-D
12.6
INT2-D
1.41
1.86
0.0
RE2-D
1.61
1.2
0.7
RE1
1.42
1.15
1.72
163.8°
16.1
15.8
14.6
TS1
1.10
2.18
1.62
158.2°
-0.9
-1.3
INT1
2.91
0.98
1.80
12.9
2.50
0.97
1.87
13.3
6.0
2.5
TS2
1.41
0.98
-39.4
-41.8
PR1
conformation switch
hydrogen abstraction
radical rebound
aromatic hydroxylation
aliphatic hydroxylation

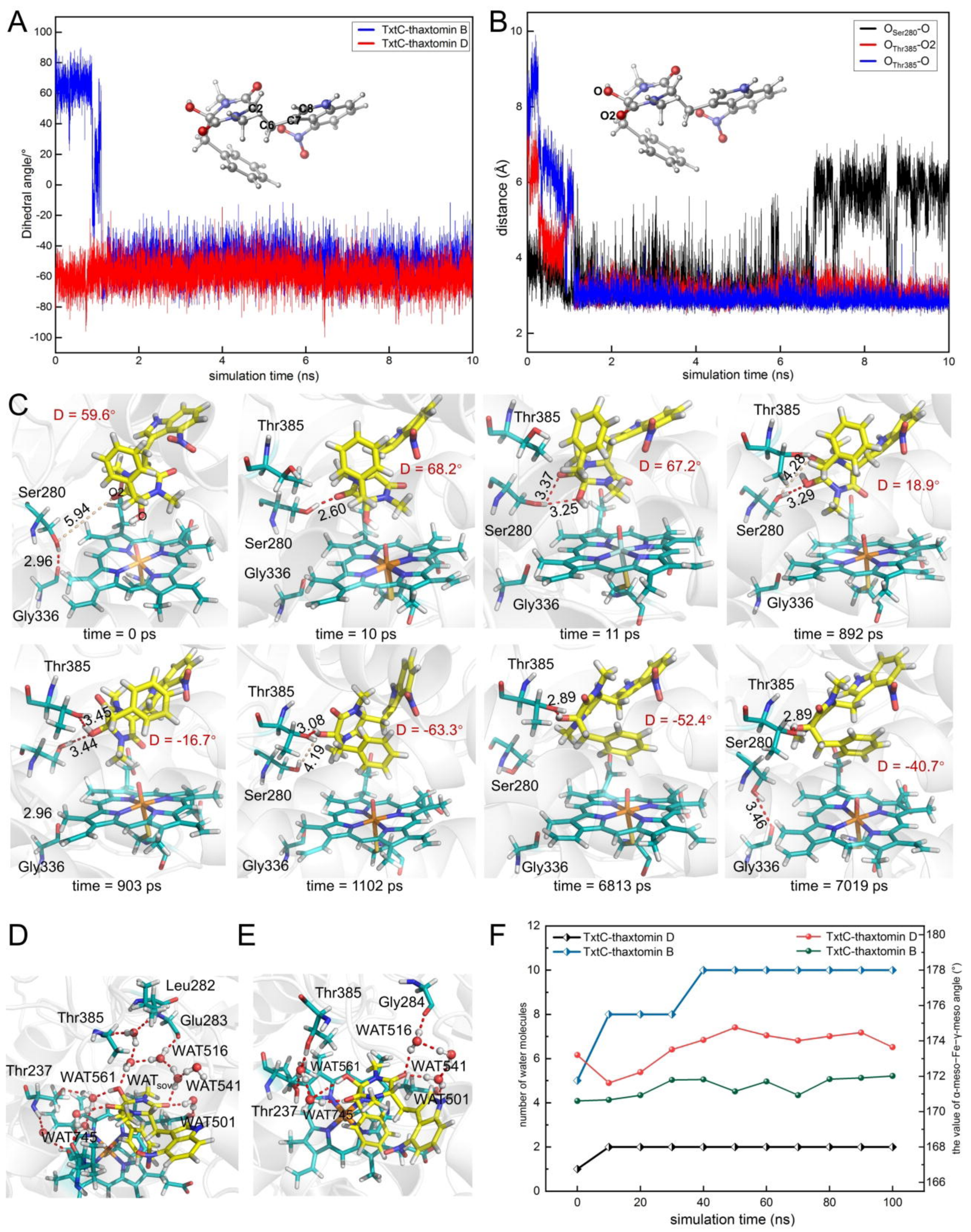
A
TxtC-thaxtomin B
TxtC-thaxtomin D
Dihedral angle/°
simulation time (ns)
C2
C6
C7
C8
B
O_{Ser280}-O
O_{Thr385}-O2
O_{Thr385}-O
O
O2
distance (Å)
simulation time (ns)
C
D = 59.6°
Ser280
O2
O
5.94
2.96
Gly336
time = 0 ps
Thr385
D = 68.2°
2.60
Ser280
Gly336
time = 10 ps
Thr385
D = 67.2°
3.37
3.25
Ser280
Gly336
time = 11 ps
Thr385
4.28
3.29
D = 18.9°
Ser280
Gly336
time = 892 ps
Thr385
3.45
3.44
D = -16.7°
2.96
Gly336
time = 903 ps
Thr385
3.08
D = -63.3°
4.19
Ser280
Gly336
time = 1102 ps
Thr385
2.89
D = -52.4°
Ser280
Gly336
time = 6813 ps
Thr385
2.89
Ser280
D = -40.7°
3.46
Gly336
time = 7019 ps
D
Leu282
Thr385
Glu283
WAT516
Thr237
WAT561
WAT_{sov}
WAT541
WAT501
WAT745
E
Thr385
Gly284
WAT516
WAT561
WAT541
WAT501
Thr237
WAT745
F
TxtC-thaxtomin D
TxtC-thaxtomin B
TxtC-thaxtomin D
TxtC-thaxtomin B
number of water molecules
the value of α-meso−Fe−γ-meso angle (°)
simulation time (ns)

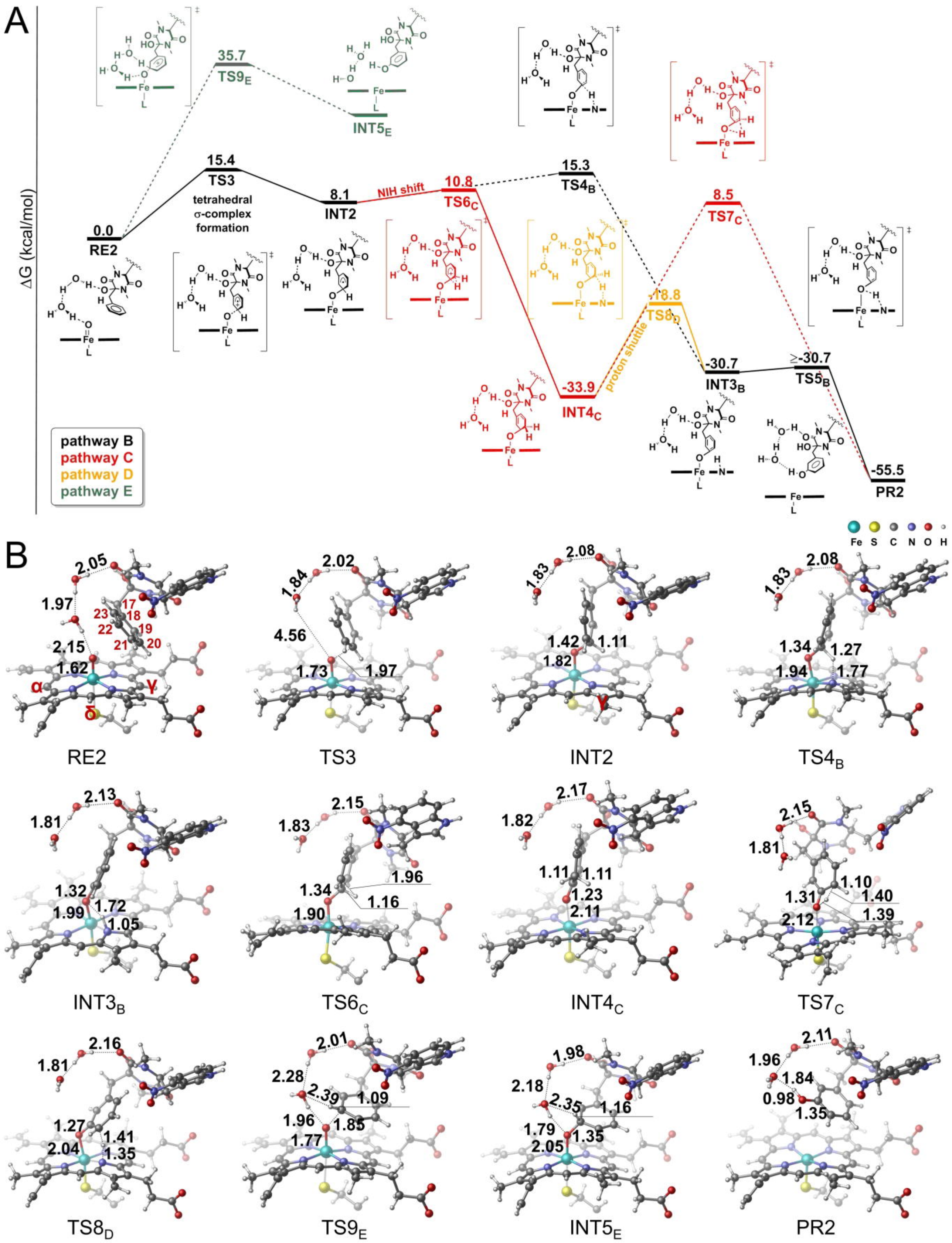
A
ΔG (kcal/mol)
0.0
RE2
15.4
TS3
tetrahedral σ-complex formation
8.1
INT2
NIH shift
10.8
TS6C
15.3
TS4B
35.7
TS9E
INT5E
-33.9
INT4C
proton shuttle
-18.8
TS8D
8.5
TS7C
-30.7
INT3B
≥-30.7
TS5B
-55.5
PR2
pathway B
pathway C
pathway D
pathway E
B
Fe S C N O H
RE2
TS3
INT2
TS4B
INT3B
TS6C
INT4C
TS7C
TS8D
TS9E
INT5E
PR2

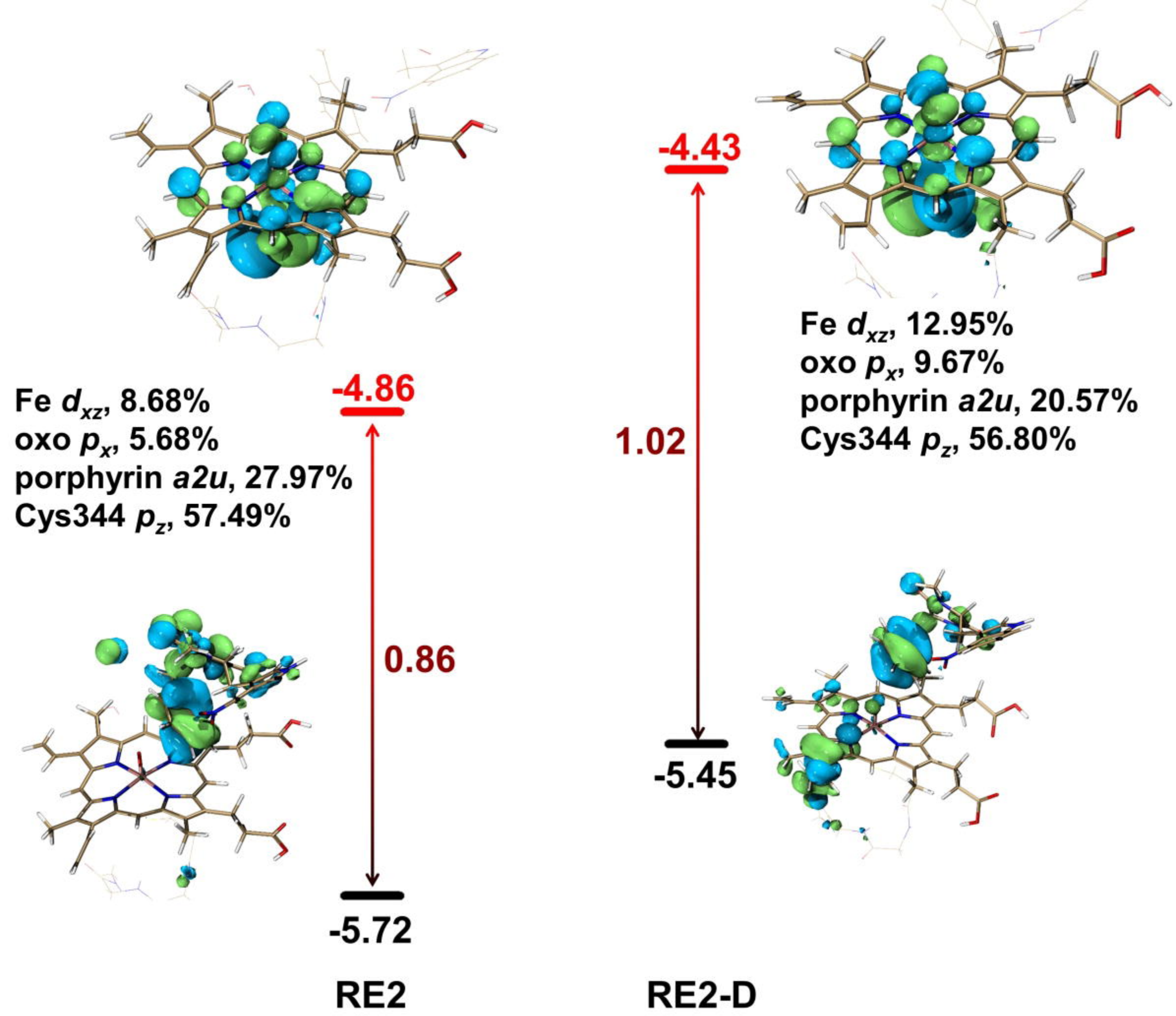
Fe d_{xz}, 8.68%
oxo p_x, 5.68%
porphyrin *a2u*, 27.97%
Cys344 p_z, 57.49%
-4.86
0.86
-5.72
RE2
-4.43
1.02
-5.45
Fe d_{xz}, 12.95%
oxo p_x, 9.67%
porphyrin *a2u*, 20.57%
Cys344 p_z, 56.80%
RE2-D

A
= porphyrin
B
L-4-nitrotryptophan
L-Phe
thaxtominD
thaxtominB
thaxtominA
TxtC
C
hydrogen abstraction
hydroxyl rebound
RE1
INT1
PR1
D
C-O breakage pathway A
Ring Closure pathway A
proton shuttle pathway A
tetrahedral σ-complex formation
proton shuttle pathway B
RE2
INT2
INT5B
PR2
tetrahedral σ-complex formation pathway E
pathway C NIH shift
proton shuttle pathway D
proton shuttle pathway C
INT6C
pathway E proton shuttle
INT7E
PR2